On the effect of the electrical load on vibration energy harvesting under stochastic resonance

Alevras, Panagiotis

DOI:
10.1115/1.4049209

Document Version
Peer reviewed version

Citation for published version (Harvard):
Alevras, P 2021, 'On the effect of the electrical load on vibration energy harvesting under stochastic resonance', *ASCE-ASME Journal of Risk and Uncertainty in Engineering Systems, Part B: Mechanical Engineering*, vol. 7, no. 1, 010902. https://doi.org/10.1115/1.4049209

On the effect of the electrical load on vibration energy harvesting under stochastic resonance

Panagiotis Alevras[1]
Department of Mechanical Engineering, School of Engineering, University of Birmingham, Birmingham, B15 2TT, UK
P.Alevras@bham.ac.uk

ABSTRACT

Vibration energy harvesting is a promising alternative for powering wireless electronics in many practical applications. Ambient vibration energy in the surrounding space of a target application often involves an inescapable randomness in the exciting vibrations, which may lead to deterioration of the expected power gains due to insufficient tuning and limited optimal designs. Stochastic resonance is a concept that has recently been considered for exploiting this randomness towards improving power generation from vibrating systems, based on the co-existence of near-harmonic vibrations with broadband noise excitations in a variety of practical mechanical systems. This paper is concerned with the optimal conditions for stochastic resonance in vibration energy harvesters, exploring the frequently neglected effect of realistic architectures of the electrical circuit on the system dynamics and the achievable power output. A parametric study is conducted using a numerical Path Integration method to compute the response Probability Density Functions of vibration energy harvesters, focusing on the effect of standard electrical components; namely, a load resistor, a rectifier and a capacitor. It is found that the conditions for stochastic resonance exhibit a nonlinear dependence on the weak harmonic excitation amplitude. Moreover, the modified nonlinear dissipation properties introduced by the rectifier and the capacitor lead to a trade-off between the power output and the non-conducting dynamics that is essential in order to determine optimal harvesting designs.

KEYWORDS: Vibration energy harvesting; bi-stable; stochastic resonance; path integration

[1] Corresponding author

1 INTRODUCTION

In recent years, Vibration Energy Harvesting (VEH) has attracted significant interest in diverse research communities as a potential alternative power source for remote wireless small electronics. Numerous sensors, microcontrollers, transceivers, etc., are being installed in traditional engineering applications to assist in the operation and control of complex systems, offering future opportunities for product refinement, wireless online condition monitoring and structural health monitoring. At present, Wireless Sensor Nodes (WSN) are primarily powered by batteries, which nonetheless, have a finite lifespan with the requirement for easy access for periodic battery replacements. This is not always an easy task that greatly increases the associated costs of the technology and, in some cases, it may even negatively affect its feasibility. VEH devices are intended to replace batteries for WSNs [1], with a nearly infinite lifespan when the stored energy is concerned and the additional benefits of sparing hazardous chemicals and of the in-situ generation of clean, green energy.

VEH devices are resonators that convert energy from mechanical vibrations to electrical energy [2] based, in their majority, on piezoelectric elements [3] or electromagnetic induction [4]. Interestingly, the normalised generic mathematical models that describe the dynamics of each of these transduction options present significant similarities, particularly in terms of the optimisation of the electric circuit. This has allowed many researchers to study both systems under an archetypal model (see for example [5]), and therefore, the results of this paper are easily extendable to each of the major transduction methods as long as the normalised parameters are properly interpreted.

Despite the attractive potential, VEH technology is limited by the need for fine tuning of the harvester's natural frequency to ensure efficient harvesting. Ambient vibrations, though, are subject to in-service variations which leads harvesters away from their design resonant point with devastating reduction of the achievable power harvesting. Researchers have recently proposed the intentional introduction of nonlinearities to overcome this shortcoming [4]-[7]. Nonlinearities trigger large response amplitudes over wide frequency ranges due to the structure of the so-called backbone curve [4] or due to other nonlinear phenomena [9], such as parametric resonance [6], multiple resonances zones [7], vibro-impact dynamics [8]. Among the various concepts proposed in the literature, nonlinear harvesters with multi-stable potential energy have been shown to offer significant improvements [10]. In particular, bi-stable harvesters exhibit two major response regimes among others. Intra-well oscillations regard trajectories with relatively low energy that are trapped within one of the potential energy wells. On the other hand, inter-well or cross-well oscillations occur as soon as the oscillator's trajectories contain enough energy to overcome the energy barrier separating the potential energy wells. Typically, cross-well oscillations lead to multiple times higher

oscillation amplitudes with respect to intra-well oscillations, with resultant improvements in the generated power [11]. The design of the parameters of the potential well, such as the well depth, and the oscillator's damping play a major role in determining the response regime for given excitation properties [12].

Often, ambient vibrations unfold as a stochastic process due to inherent randomness and uncertainties, requiring advanced probabilistic treatment, particularly for nonlinear VEH [13]. The joint PDF of nonlinear oscillators is particularly difficult to obtain analytically apart from certain exceptions. To overcome this, computational and approximate analytical methods are used to study in detail the stochastic dynamics of nonlinear oscillators ([8],[13]-[14]). Cross-well oscillations of bi-stable energy harvesters have also been proposed for combined harmonic and stochastic excitation [15]. McInnes et al [15] proposed the utilisation of Stochastic Resonance (SR) [16], a concept which involves the amplification of a weak harmonic force under a superimposed broadband noise. In a VEH context, the combined action of the weak harmonic excitation with noise leads to enhanced power output under resonance-like prescribed forcing conditions, where each of the individual excitations would be insufficient to establish cross-well oscillations. Experimental verification of the application of SR in VEH has been demonstrated by Zheng et al [17] using a piezoelectric beam with a set of a tip magnet and a static facing magnet providing the bi-stable potential energy. Many researchers have studied the benefits of SR for VEH, particularly in rotational applications, where harmonic excitation is inherently linked with the kinematics of rotary equipment [18]-[23].

Recently, the effect of ambient randomness on VEH has been studied via the stochastic averaging technique [24]-[25], which has been extended to bi-stable VEH as well [26]. Yang et al used stochastic averaging to study the effect of static and periodic modulations on a generic electromagnetic bi-stable VEH concept. Liu et al [28] investigated the effect of noise filtering on the statistical properties of the harvester's power, whereas Zhang et al [5] and Zhang et al [29] explored the benefits of tri-stable oscillators using stochastic averaging. However, the majority of these studies adopted a simplified version of the electric circuit, which typically considers only purely resistive elements to close the electric circuit. Randomness in the vibrations source and the fundamental oscillatory excursion of this energy source, lead to AC induced voltages with frequently varying characteristics. Utilization of the generated electricity to power small electronics, such as wireless sensors, should conform to practical standards, which prescribe a DC voltage input for this type of electrical loads. Therefore a rectifier is essential to convert the generated AC voltage to a standard DC signal. Consequently, a stabilising capacitor is also necessary to mitigate voltage fluctuations, which could be used for energy storage as well. Realistic circuits have been considered in terms of

power management issues [30] and scarcely for response bandwidth considerations [31]-[33]. However, the discontinuous current flow and the strong in-cycle nonlinearities lead to modified electrical dissipation for the mechanical oscillator, which may have a direct impact on the optimal conditions for SR.

Dai and Harne [30] used an equivalent linearization method to study SR for an experimental demonstration of the concept for VEH. This work provided significant insights on the impact of the rectifier-capacitor on the VEH efficiency under combined harmonic and stochastic excitation. The same authors have extended this work to study the conditions for optimal DC power delivery, exploring issues of optimal resistance [33]; This paper focuses on the effect of standard architectures of the electric circuit on the establishment of SR and the associated impact on the generated power. Section 2 introduces an archetypal model of bi-stable electromagnetic VEH in three steps of increasing complexity, starting from purely resistive loads and progressively considering the impact of rectifiers and capacitors. Moreover, a brief description of the concept of SR is provided for completeness and for easing the reader, whereas the background motivation for this paper is showcased via selected random samples. The stochastic models are thoroughly analysed using the computational power of a numerical Path Integration (PI) approach, which is described in Section 3. Numerical results of the nonlinear oscillator's mean crossing rates over the potential well barrier and the corresponding power output are shown in Section 4, based on the individual joint response PDFs. Finally, the major conclusions of this paper are summarised in the end.

2 GENERIC ELECTROMECHANICAL ENERGY HARVESTER

2.1 Mathematical models

Let us consider a generic vibration energy harvester as it is depicted in the sketch shown in Fig. 1. Among the very diverse harvesting concepts that have been proposed in the literature in recent years, one can identify similarities in the construction of the mathematical models that are used to study the response of these electromechanical systems to exciting vibrations. Specifically, VEHs are modelled as (nonlinear) mechanical oscillators coupled with an electric circuit, whereby coupling of the two sub-systems is typically realized through a linear term modelling the induced voltage and the exerted Lorenz force. Therefore, the analysis that follows is relevant to a broad range of concepts that are designed to operate under stochastic resonance.

Figure 1.

The VEH shown in Fig. 1 can be modelled using the governing equations shown in Eq. (1) [30]:

$$\begin{gathered} m\ddot{x} + c_m\dot{x} - kx + k_3x^3 + \kappa I = m\ddot{x}_b \\ L\dot{I} + R_wI + V_L = \kappa\dot{x} \end{gathered} \tag{1}$$

where the first equation describes the dynamics of the mechanical oscillator and the second one the dynamics of the electric circuit. In Eq. (1), m is the oscillator mass, c_m is the mechanical damping coefficient, k is the linear stiffness coefficient, k_3 is the nonlinear stiffness coefficient, κ is the electromechanical constant, I is the electrical current, x_b is the base excitation, L is the coil's inductance, R_w is the coil's electrical resistance, also referred to as internal resistance, whereas V_L is the voltage across the electrical load that the VEH is intended to supply power to.

Typically, mechanical vibrations involve frequencies which render the influence of inductance negligible with respect to the resistive loads, i.e. $\omega L \ll R_w + R_L$, which simplifies the second equation in an algebraic form. Let us now manipulate Eq. (1) to reduce it to a normalized form, neglecting the inductive term. First, we normalise the oscillator's coordinate with a length scale $l_c = \sqrt{(k/k_3)}$ by defining $z = x/l_c$ and we adjust the time of the system to $\tau = \omega_n t$, where $\omega_n = \sqrt{k/m}$. Applying these transformations leads to the following:

$$\begin{gathered} z'' + 2\zeta_m z' - z + z^3 + \frac{\kappa I}{k l_c} = z_b'' \\ R_wI + V_L = \kappa\omega_n l_c z' \end{gathered} \tag{2}$$

where the base excitation has been scaled with l_c as well. At this point, we shall distinguish three architectures for the electrical loads that will accompany the remaining sections of this paper [30]. Even though researchers have previously considered purely resistive elements in the form of electrical damping, these studies have been limited in optimizing the load under single frequency excitations. Furthermore, we shall investigate the effect of non-resistive components on the conditions that allow the establishment of stochastic resonance via direct comparison.

Case I: Series resistive load

A large majority in the literature concerning VEHs has treated the electrical load as a simple resistive element, connected in series with the exciting coil. With this assumption, the load voltage is expressed as $V_L = I\,R_L$, which if substituted in the second equation of Eq. (2), leads to an expression for the electrical current, $I = \kappa\omega_n l_c z'/(R_w + R_L)$. Substituting the expression for the current in Eq. (2), one is led to the following SDOF governing equation. Note that the base acceleration has been replaced by a harmonic term and a delta-correlated

Gaussian white noise, $\xi(\tau)$, for which $\langle \xi(\tau)\xi(\tau+s)\rangle = D\delta(s)$ with $D=\sigma^2$ denoting the noise intensity:

$$z'' + 2(\zeta_m + \zeta_e)z' - z + z^3 = A_n \cos\omega\tau + \xi(\tau) \tag{3}$$

where the electrical damping coefficient given by $c_e = \kappa^2/(R_w + R_L)$ has been used to define an equivalent electrical damping ratio as in $\zeta_e = c_e/c_{cr}$ and the critical damping given by $c_{cr} = 2\sqrt{km}$. This approach essentially reduces the dimension of the problem since the contribution of the electric circuit to the system dynamics is then limited to a passive electrical damping term. The above simplification has been used by many researchers in the literature, particularly in studies that are concerned with stochastic analyses of the power harvested by vibrations, due to the favourable mitigation of expensive computations which is rather pertinent in such analyses. In this paper, Case I is used to initially explore the frequency conditions that may lead to stochastic resonance. The system in Eq. (3) has been the basis for the to-date development of harvesters exploiting stochastic resonance and, as such, it may serve as a baseline for the herein investigations. Note that the normalised mean power in this case is given by $P_L = I^2R_L/\kappa^2\omega_n^2 l_c^2 = r^2 z'^2/R_L$ to ease later comparison.

Case II: Rectifier and resistor

Typically, low-power electronics, such as those targeted in VEH applications, are standardized to accept DC voltage inputs. When a simple ideal resistor closes the coil circuit as in Case I, the induced voltage has an alternating profile following the vibrations of the mechanical oscillator. This creates the need to convert the AC induced voltage to a DC signal that is suitable for powering the electrical load. The most common approach is to use a typical diode bridge rectifier circuit in between the coil and the load, as it is shown in Fig. 1(c). Bridge rectifiers allow one way flow of current thus converting the generated alternating voltage to a DC signal that is suitable for the considered applications.

Nevertheless, diodes introduce a voltage drop which depends on the semiconductor material that is used. When the induced voltage is less than the diode threshold V_r, the rectifier is off and the harvester works in open circuit. Correspondingly, when the voltage overcomes the threshold the rectifier is turned on and current flows in the load. Typical values for this threshold range from 0.2 V (Schottky diodes) up to 0.7 V (silicon diodes). This effectively acts as an on-off switch within each vibration cycle depending on the induced voltage, leading to highly nonlinear trajectories with characteristically nonlinear damping properties. From the mechanical oscillator's viewpoint, the off state leads to less energy dissipated and consequently higher kinetic energy is stored in the oscillator. On the other hand, the on-off

operation leads to power being harvested only within a proportion of the cycle, thus reducing the vibration energy that is converted to electricity. When a rectifier is interposed, the governing equations in Eq. (2) take the following form:

$$\begin{aligned} &z'' + 2(\zeta_m + \zeta_e)z' - 2\zeta_e U_r \mathrm{sgn}(z') - z + z^3 = A_n \cos\omega\tau + \xi(\tau) \qquad \text{when } |z'| > U_r, \\ &U_L = r|z'| - rU_r \\ &z'' + 2\zeta_m z' - z + z^3 = A_n \cos\omega\tau + \xi(\tau) \qquad \text{when } |z'| \le U_r \\ &U_L = 0, U_{OC} = z' \end{aligned} \tag{4}$$

Where the voltage threshold has been normalized to $U_r = V_r/(\kappa\omega_n l_c)$ and the load voltage to $U_L = V_L/(\kappa\omega_n l_c)$. Using these transformations, the condition for the rectifier to conduct, i.e. $V_{OC} > V_r$, is expressed in terms of the non-dimensional velocity z'. Apart from the impact of the on-off operation on the overall system damping, one may observe that the voltage threshold is also reducing damping in the "on" state, through a negative dry friction term that arises in the oscillator's equation of motion. This complicated response raises the question of the impact of the rectifier and its threshold on the conditions that can lead to cross-well oscillations under combined deterministic and stochastic excitation. The rectifier affects the continuity of the harvested power, which is given by $P_L = (V_L^2/R_L)/\kappa^2\omega_n^2 l_c^2 = U_L^2/R_L$ when the rectifier conducts, and $P_L = 0$ when the circuit is open.

Case 3: Rectifier, capacitor and resistor

A characteristic drawback of rectifiers is the so-called rippling output, on top of the voltage drop. Full-wave rectifiers essentially mirror the negative part of the induced voltage to the positive semi-axis, essentially leading to a load input with a persisting fluctuating profile. This is counteracted by the additional integration of suitable capacitors in the output of the rectifier, as it is shown in Fig. 1(d). Even though the rippling effect is still present, the capacitor charge greatly reduces its magnitude. Proper sizing of the capacitance not only minimizes the voltage fluctuations, but it may ensure continuous supply of voltage to the load when the rectifier is off. Largely, this parallel RC circuit can effectively convert the alternating harvested voltage to a nearly DC signal. When a capacitor is introduced, the system is described by two differential equations, given by:

$$z'' + 2\left(\zeta_m + \frac{\zeta_e}{1-r}\right)z' - \frac{2\zeta_e(U_r + U_L)\mathrm{sgn}(z')}{1-r} - z + z^3 = A_n \cos\omega\tau + \xi(\tau)$$
$$U_L' = r\alpha(|z'| - U_r) - \alpha U_L\,, \qquad |z'| > U_r + U_L$$

and

(5)

$$z'' + 2\zeta_m z' - z + z^3 = A_n \cos\omega\tau + \xi(\tau), \qquad |z'| \le U_r + U_L$$
$$U_L' = -\delta U_L$$
$$U_{OC} = z'$$

where the following parameters have been defined: $\alpha = 1/r\omega_n R_w C_r$ controlling the circuit's impedance and $\delta = 1/\omega_n C_r R_L$ representing the capacitor's discharge rate. In what follows, Eqs (3)-(5) will be the basis for investigating the excursion of stochastic resonance in Cases I – III and the attached implications for the harvested power.

2.2 Stochastic resonance

Consider a general bi-stable mechanical oscillator under combined harmonic and wideband stochastic excitation, the dynamics of which are governed by a differential equation similar to Eq. (2) if the electrical damping, ζ_e, is dropped. The potential energy of this oscillator $U(z) = -z^2/2 + z^4/4$ involves two minima (stable equilibria) and a local maximum (unstable equilibrium) at $z = \pm 1$ and $z = 0$ respectively. The shape of $U(z)$ formulates two potential wells where the oscillator is trapped if the excitation intensity is small. The depth of the symmetric potential wells, $\Delta U = |U(0) - U(1)| = 1/4$, defines a barrier that the oscillator has to overcome to transit from one well to the other. Combining a weak harmonic excitation with a low-intensity stochastic excitation ($D \ll \Delta U$) has been shown to trigger random transitions between the potential wells [16], even when each of the excitations alone would lead to intra-well oscillations trapped by the potential barrier.

Figure 2.

The above phenomenon is referred to as stochastic resonance in the literature, since cross-well response is initiated by the superposition of low-intensity noise on periodic modulations of the potential energy. Essentially, SR leads to cross-well oscillations which have been extensively studied for VEH due to the high vibration amplitude compared with their mono-stable counterparts. The application of the weak harmonic excitation periodically modulates the potential energy function and the crossing barrier imposed by the corresponding potential depth (see Fig. 2). When the noise is synchronized with this modulation in the mean

sense, the oscillator jumps between the potential wells leading to the establishment of cross-well vibrations. This synchronization occurs when the average waiting time of the oscillator in a potential well is half the period of the harmonic excitation, $\tau_s = 2\,\tau_w$, or expressed in frequencies, $\omega_s = \pi r_k$, where r_k is the transition rate between the two potential wells given by the well-known Kramer's rate [34]:

$$r_k = \frac{1}{\sqrt{2}\pi} e^{\left(-\frac{\Delta U}{D}\right)} \tag{6}$$

Consequently, the condition for stochastic resonance has been expressed as

$$\omega_s = \frac{1}{\sqrt{2}} e^{\left(-\frac{\Delta U}{D}\right)} \tag{7}$$

However, Kramer's rate has been developed for the crossing problem of overdamped particles. Application of Eq. (7) in the herein described problem would lead to extremely low values due to the exponent and the assumed weakness of the noise intensity with respect to the barrier. Previous applications of SR in the literature concerned with VEH have used the limit of Eq. (7), as in $\omega_{s,l} = 1/\sqrt{2}$, to overcome this deficiency (such as in [17]). Note that according to Eq. (7), $\omega_{s,l}$ is also the maximum value that the frequency condition can attain. Although a limited number of works has extended this analysis to an underdamped version of Kramer's rate following the deepest descent method [27], this has been shown it is less accurate than alternative methods such as Melnikov's method [35]. Nevertheless, even though experimental verification of SR under this forcing condition has been provided (e.g. [17],[35]), the application breadth of the above assumptions is unclear. As a demonstration, consider the responses shown in Fig. 3, concerning a bi-stable oscillator described by Eq. (2) and initially at rest at $z = 1$. Figure 3(a) shows the steady-state deterministic phase space plot when the noise is cancelled and for $\omega = \omega_{s,l} = 0.707$, clearly leading to an intra-well attractor. Correspondingly, when only the stochastic term excites the oscillator, the response in Fig. 3(b) is mostly trapped within the potential well. Of course, given the wideband property of the forcing term, one cannot exclude the possibility of crossings, however this can only be realised at very slow crossing rates. When both the weak harmonic and the stochastic terms are combined in Fig. 3(c), the oscillator clearly jumps from one well to the other at a frequent rate, which is a manifestation of SR. Note that this response is extracted at $\omega_{s,l}$, which has been assumed to be the maximum (and most favourable) frequency that SR can occur. Nevertheless, if one considers higher frequencies such as up to $\omega_s = 1$, the oscillator continues to perform cross-well oscillations under the combined influence of the examined excitation, and noteworthy, at increasing rates. This is clearly evident in Fig. 3(c)–(f) where,

as the harmonic frequency is increased, the random response is progressively attracted more and more by the inter-well vibrations, up to the point that it almost exclusively jumps between the wells when $\omega = 1$. Furthermore, this increase in the crossing rate cannot be attributed to a deterministic resonance due to the harmonic term, as the deterministic response to this frequency would still be confined in the initiating well, as Fig. 3(a) shows. Consequently, optimal design of a vibration energy harvester to fully exploit the benefits of SR is subject to the above observation. Conversely, one cannot generalise these observations simply based on one realisation of the stochastic response. A formal probabilistic analysis is required in order to understand the benefits of SR for VEH beyond Kramer's rate. The following analysis first investigates the effect of the harmonic frequency on the manifestation of SR and afterwards, the role of electrical damping is explored for common architectures of the electric circuit, which implicates the electrical parameters and the induced current flow. A parametric study is conducted in the following sections based on numerically calculating the Probability Density Function (PDF) of the harvester response in Cases I – III. The PDF is computed via a numerical PI technique, which is briefly described in the next section.

Figure 3

3 PATH INTEGRATION

The generic vibration energy harvester models presented in the previous section are studied using a numerical PI method to compute the transient and stationary joint response PDF of the harvesters described by Cases I – III. Path Integration has been used to compute the response PDF of strongly nonlinear oscillators with numerical ([36]-[38]) and analytical schemes ([39]-[40]). In fact, the method has been previously used to analyse nonlinear mono-stable harvesters with hardening springs [39]. Knowledge of the PDF of the mechanical and electrical variables z, z' and U_L can provide superior probabilistic information compared with approximate techniques such as stochastic averaging that has been widely employed in the past. In fact, the PI approach can reach accurate expressions for the tails of the PDF which are closely related to rare events. Moreover, one can extend the analysis of the harvesting systems beyond the stationary solution.

The numerical PI method involves an iterative approach to numerically propagate the probability flow of a vibrating system in short time steps, exploiting the assumption that the unknown stochastic process has very short memory with respect to the system dynamics, i.e. the Markov property is satisfied. Essentially, the method receives an input of initial conditions in the form of an initial PDF, which is then propagated forward in time until a stationary solution is reached or until the sought transient probabilistic information is collected. This

method has been developed as an alternative to finite element methods solving the FPK equation, which often involve excessive computational cost.

Consider, then, the following stochastic differential equation on an n-dimensional Ito process $\boldsymbol{X}$:

$$\dot{\boldsymbol{X}} = \boldsymbol{a}(\boldsymbol{X}, t) + \boldsymbol{b}(\boldsymbol{X}, t)\boldsymbol{Z} \tag{8}$$

where $\boldsymbol{a}$ is the drift matrix and $\boldsymbol{b}$ the diffusion matrix, $\boldsymbol{Z}$ is an m-dimensional vector of independent Gaussian white noise stochastic processes. Adapting this to the herein examined cases, let us assume that the noise process is one-dimensional, and entering the system dynamics only through the n-th equation. Therefore, $\boldsymbol{b}$ becomes a vector, for which $\boldsymbol{b}^T = [0 \dots \sigma]$. The PI method is fundamentally based on the total probability law, which in the case of a Markov process reads:

$$p(\boldsymbol{x}(t_2), t_2) = \int_{-\infty}^{\infty} p(\boldsymbol{x}(t_2), t_2 | \boldsymbol{x}(t_1), t_1) p(\boldsymbol{x}(t_1), t_1)\, d\boldsymbol{x}_1 \tag{9}$$

where it has been assumed that $t_2 > t_1$. The numerical implementation of Eq. (9) requires an assumed input of $p(\boldsymbol{x}(t_1), t_1)$ as the initialisation of the computational problem and an expression for the Transitional Probability Density Function (TPDF), $p(\boldsymbol{x}(t_2), t_2 | \boldsymbol{x}(t_1), t_1)$. The latter function has been proven [38] to adopt a degenerate multivariate Gaussian distribution if the execution time step is sufficiently small, which is typically true in relevant numerical algorithms. Therefore, the TPD takes the following form:

$$p(\boldsymbol{x}_2, t_2 | \boldsymbol{x}_1, t_1) = \prod_{i=1}^{n-1} \delta(x_{i,2} - x_{i,1} - r_i(x_{i,1}, t_1, \Delta t)) \hat{p}(x_{n,2} | \boldsymbol{x}_1) \tag{10}$$

Where

$$\hat{p}\left(x_{n,2} \middle| \boldsymbol{x}_1\right) = \frac{1}{\sqrt{2\pi D \Delta t}} \exp\left\{ - \frac{\left[x_{n,2} - x_{n,1} - r_n(\boldsymbol{x}_1, \Delta t)\right]}{2 D \Delta t} \right\} \tag{11}$$

Where $r_j, j = 1 \dots n$ denotes the deterministic 4th-order Runge–Kutta integration step from $x_{n,1}$ to $x_{n,2}$ at a time step of Δt, $D = \sigma^2$ is the noise intensity and $\delta(\cdot)$ denotes the Dirac-delta function. Equations (10) and (11) are closed form expressions which provide the transition

characteristics of the probability flow that are necessary to compute $p(\boldsymbol{x}_2, t_2)$. The equations of motion described by Eq. (2) and the individual cases represented by Eqs (3)-(5) are used to calculate the deterministic Runge-Kutta paths, r_j, by expressing them as a first order vector differential equation. Note that the PI method entails the computation of the joint response PDF at state space points that are generally not equal to the pre-defined mesh points that are used to discretize the state space. Therefore, an interpolation scheme is necessary in order to compute the PDF values at any arbitrary point of the system's state space. In this paper, and given the relatively low computational requirements of the considered problems, cubic B-splines are used to improve accuracy of the method.

Iterative application of Eqs (9)-(11) leads to the calculation of the joint PDF at an arbitrary time. Nevertheless, the PI method suffers from the so-called curse of dimensionality alike most mesh-based computational methods, which presents a challenge when higher order vibrational systems are concerned. Fortunately, the vibration energy harvesters that are considered in this paper involve relatively low dimensions, which makes the application of this version of PI computationally manageable.

4 NUMERICAL RESULTS

A numerical parametric analysis is conducted to reveal the influence of the components of the electrical circuit on the establishment of stochastic resonance and the achievable conversion of vibrations to electrical power. The complexity of the electric circuit is gradually increased following the Cases I-III presented in Section 2 to individually focus on the effects of the resistive load, the rectifier and a stabilizing/storage capacitor respectively. The generic stochastic models in Eq. (3)-(5) are treated with the numerical PI method described in the previous section to extract the joint PDF of each system's response. In order to track the establishment of stochastic resonance, we monitor the evolution of bi-directional crossings from one potential well to the other. This is achieved by computing the mean crossing rate through the potential barrier at $z = 0$. Knowledge of the joint response PDF of the kinematic variables z and z' acquired by the PI method readily allows computation of the crossing rate via:

$$\nu_{r\pm} = \int_{z'} |z'| p_{zz'}(z = 0, z')\, dz' \tag{12}$$

where the absolute value is used to account for crossings in both directions. To simplify the crossing rate notation, the $\pm$ subscript will be omitted from here onwards.

4.1 Resistive load

The analysis first considers Case I whereby a purely resistive electrical load closes the circuit in series with the coil (Fig.1(b)). This is the most simplified version of the system dynamics, which has, nevertheless, been used by the majority of researchers to study the harvesting potential of various concepts. Herein, this simplified model is used to explore the impact of the weak excitation frequency on the conditions for stochastic resonance, following the preliminary discussion stemming from Fig (3) that highlighted the observation that the sought resonance can potentially be stronger and more robust at frequencies different from those given by Kramer's rate.

Picking up the thread from the sampling results in Fig. 3, the joint response PDF is computed via the PI method using the same parameters that led to the results shown in Figs 3(d) and 3(f), i.e. for $\omega = 0.7$ and $\omega = 1.0$ respectively. The joint PDFs for these two case studies are plotted in Fig 5. Evidently, the tentative observation that the frequency close to Kramer's rate leads to weaker resonance with less frequent jumps between the two potential wells is confirmed by the full probabilistic information contained within the stationary PDF. A homoclinic orbit separates the state space in two major parts: the outer one that leads to trajectories performing cross-well oscillations and the inner one where the oscillator is trapped within the corresponding well and performing in-well oscillations around its equilibrium. With regards to the state space view of the PDFs shown in Fig 4, trajectories outside this homoclinic orbit contain enough energy to overcome the potential barrier and are therefore more likely to jump to the other well along their path. Consequently, stochastic resonance with robust crossings between the two wells is reasonably expected to drive the probability density towards the cross-well trajectories outside the homoclinic orbit. Looking at the color-coded PDFs at Fig 4, when $\omega = 0.7$ the majority of the density is concentrated around the two stable equilibria implying a tendency of the system to vibrate within each well with infrequent crossings. On the other hand, Fig 4(b) clearly shows that the cross-well trajectories attract significantly higher part of the probability density, leading to higher probability for crossings, which may act as an indication for SR. This is also evident in the marginal PDFs of the oscillator's displacement and velocity in Figs 4(c) and 4(d), where the central part of the displacement density involves relatively high values, pointing towards increased rate of crossings. Note that the marginal PDFs are also compared with MC simulations of 1,000 samples as validation of the accuracy of the applied computational method.

Figure 4

Overall, computation of the joint PDF with the PI method has reaffirmed the tentative observations originating from the results in Fig. 3. In order to put this observation in a quantitative context a wide parametric study is conducted using the PI computation of the joint response PDF, monitoring the crossing rate given by Eq. (12). Fig. 5(b) shows the moving average of the crossing rate for two case studies where the sets of parameters are chosen in a similar way that highlights the impact of the excitation frequency. Note that the moving average is used to reduce the crossing rate to a single value per time instance for comparison, given that the periodicity of the weak harmonic force leads to periodic variations of the crossing rate as it is shown in Fig. 5(a). The crossing rate shows a noteworthy improvement for the frequency chosen to be the furthest apart from the previously used frequency condition based on Kramer's rate. The crossing rate when $\omega = 0.9$ is around four times the corresponding rate at $\omega = 0.75$. This essentially implies that the harvester would spend, on average and when stationary conditions have been reached, four times longer time on cross-well oscillations which are highly favourable for VEH with respect to their in-well counterparts.

Figure 5

A broader picture of the system dynamics and the relationship between stochastic resonance and the harmonic frequency can be given by constructing frequency response curves of the mean crossing rate. The crossing rate is computed across a wide frequency range, $\omega = [0.5, 1.5]$ for various values of the harmonic amplitude, A_n, until the PDF reaches stationarity and, thereafter, the average value over one excitation period is recorded and plotted in Figure 6 for comparison. Alongside the crossing rate, the mean power output delivered to the electrical load is calculated, using the mathematical expressions pertaining to Case I. Evidently, the mean crossing rate is not resonating at the previously assumed $\omega = 0.707$. This is only true for very weak amplitudes, which, nevertheless, have a minor importance for energy harvesting due to the very low achieved rate of crossings. As the excitation amplitude is increased the maximum crossing rate, i.e. resonant conditions, occurs at higher frequencies. This is very similar to the hardening behaviour of nonlinear springs. In fact, the parametric analysis in Fig. 6 shows that a locus analogous to the so-called backbone curve is forming, connecting the maxima of the plotted curves. A similar trend is observed when the mean power output is concerned, shown in Fig. 6(b). In fact, the initial assumption that tracking the mean crossing rate could essentially relate to the harvested power is reaffirmed. This highlights the nonlinear dependence of the conditions for stochastic resonance on the overall energy of the vibrating system, which can potentially have significant implications for the optimal design of vibration energy harvesters based on stochastic resonance. Although this analysis regards a simplified version of an energy harvester model, the effect of the

excitation frequency and the overall system energy on the conditions for SR points towards the relationship between damping and the input excitation amplitude as a factor for determining a harvester's optimal design. Recalling that the presented results regard normalised quantities, this effect is particularly important in relatively stiff applications where the reported difference in the optimal frequency can take values at the scale of tens of Hz.

Figure 6

We also note that this is an effect that originates from the structure of the system's conservative dynamics. If one were to examine the effect of increasing noise-to-damping ratio, a distinctively different picture is obtained. Figure 7 shows a similar parametric analysis as the one that is shown in Fig 6, only that the noise intensity is gradually increased for a fixed harmonic amplitude. The diffusing effect of noise quickly overtakes any tendency of the resonance curve to be shifted towards higher frequencies. Although the maximum crossing rate and the corresponding power output do indeed preserve a dependence on the excitation frequency, its impact on the optimal design of a vibration energy harvester is far less important.

Figure 7

4.2 Rectifier with a resistive load

The results in Section 4.1 have indeed elucidated a nonlinear dependence of the conditions for SR on the harmonic excitation frequency and the overall system energy. However, the structure of the electric circuit was excruciatingly simplified. A step towards a more realistic representation is added in the system complexity by interposing a rectifier between the coil and the load, leading to the models given for Case II.

Full wave diode bridge rectifiers conduct current unidirectionally, effectively converting AC voltage to DC, which is necessary for powering small electronics. However, rectifiers come with an efficiency which is represented by their voltage drop, V_r. This ranges from 0.7 V for silicon diodes down to 0.2 V for germanium diodes and Schottky diodes. The voltage drop modifies the damping properties of the harvester within each cycle leading to a highly nonlinear problem which involves lightly damped dynamics when the rectifier is off and stronger damping forces when the rectifier conducts and power is generated. This leads to higher probability for jumps between the two wells when the voltage threshold increases, as Fig. 8(a) shows. Three values of the normalised threshold U_r are considered and the frequency response of the crossing rate is plotted. Firstly, one may observe that the threshold has a very minor effect on the optimal frequency, which is very close to the frequency obtained by Case I. However, the modified dissipation characteristics cause substantial

differences in the expected value of the crossing rate. Although in Case I this would imply better harvesting performance, the presence of the rectifier limits the trajectories from which electrical energy is extracted. The reduced damping and the limitation of harvesting within a proportion of the trajectories leads to the combined effect on the mean power shown in Fig 8(b). Contrary to Case I, increasing crossing rates (as the voltage drop increases in magnitude) are accompanied by a reduction of the mean extracted power due to the complicated balance between the lower dissipation properties of the non-conducting trajectories and the associated load current blocking.

A closer investigation of the damping properties reveals that the optimal load is subject to the realised diode voltage drop. Figures 8(c) and 8(d) show the crossing rates and the normalised mean power ($\langle P \rangle / \langle P \rangle_{max}$) for various values of the load resistance that controls the electrical damping. Note that the power is expressed in this way since the intermittent voltage in the load would lead to a misleading comparison in absolute numbers. Moreover, a comparison based on the absolute power output would be less informative than exploring the effect of the rectifier on the optimal load. However, this problem will be addressed by the addition of a capacitor in the next section.

A well-known proven approach based on the Case I dynamics would suggest that the optimal load should match the mechanical damping coefficient. This is true for low thresholds as energy dissipation converges to Case I. Nevertheless, as the voltage drop increases leading to lighter overall equivalent damping, the optimal load needs to be adjusted to the corresponding equivalent damping. In fact, Fig 8(d) shows that the diodes with higher voltage drop lead to reduced optimal load resistance, which is consistent with the overall weaker damping forces. Note also that the rectified power is more robust with respect to its optimal load. The baseline Case I results in Fig. 8(d) show that the power output drops faster when the electrical load deviates from its optimal value. Increasing U_r on the other hand leads to more balanced power output with respect to the electrical load resistance.

However, the present architecture has been used only to explore the impact of the voltage drop on the harvested power, since the excessive voltage ripples in the output side of the rectifier would make it an unviable option. This problem can be solved by adding a parallel stabilising capacitor, which is investigated in the next section. The capacitor would also ensure continuous supply of voltage to the load.

Figure 8

4.3 Rectifier with a capacitor and a resistive load

When a capacitor is added to the output of the rectifier in parallel the harvester dynamics are governed by Eq. (5). The analysis using the PI technique in this case leads to disproportionally high computational cost due to the discontinuity in the z', U_L state space. In order to mitigate this, Eq. (5) is further simplified using the generalised harmonic functions for the displacement and velocity. This procedure has been employed for energy harvesting oscillators in the past, particularly when a stochastic averaging approach is used. Following Zhang et al [41], the differential equation of the voltage in Eq. (5) for conducting rectifier can be solved assuming a slow varying amplitude and frequency of the mechanical oscillator to give the steady state solution:

$$U_L = r\alpha\left(\frac{\alpha}{\omega_s(H)^2+\alpha^2}z' + \frac{\omega_s(H)^2}{\omega_s(H)^2+\alpha^2}(z-z_{eq})\right)sgn(z') - rU_r \qquad (13)$$

where $\omega_s(H)$ is the energy-dependent frequency of the oscillator and H its total mechanical energy. In the above approximate equation, it has been assumed that the contribution of the displacement z to the sign of the open circuit voltage is weak enough to be neglected, recalling that this analysis is carried out under the condition $|z'| > U_r + U_L$. Substituting this in the first equation in Eq. (5) and simplifying we get:

$$\begin{aligned} &z'' + 2[\zeta_m + D_e]z' - 2\zeta_e U_r \mathrm{sgn}(z') - (1+A)z + Az_e + z^3 = A_n\cos\omega\tau + \xi(\tau), && |z'| > U_r + U_L \\ &\text{and} \\ &z'' + 2\zeta_m z' - z + z^3 = A_n\cos\omega\tau + \xi(\tau), && |z'| \le U_r + U_L \\ &U_L' = -\delta U_L \\ &U_{OC} = z' \end{aligned} \qquad (14)$$

with

$$D_e\big(\omega_s(H)\big) = \frac{\zeta_e}{1-r}\left(1 - \frac{\alpha^2 r}{\omega_s(H)^2+\alpha^2}\right)$$

$$A\big(\omega_s(H)\big) = \frac{2\zeta_e r\alpha}{1-r}\frac{\omega_s(H)^2}{\omega_s(H)^2+\alpha^2} \qquad (15)$$

$$z_e = \begin{cases} \pm 1, & H < H_{hom} \\ 0, & H \ge H_{hom} \end{cases}$$

The functionals in Eq. (15) give rise to an energy-dependent damping ratio and a modulation of the potential energy. In the previous two cases, the overall resistance (internal and load) would control the magnitude of the electrical damping ratio with an inversely proportional relationship. This attribute leads to optimisation of the load resistance, such that the electrical damping matches the mechanical one. However, $D_e\big(\omega_s(H)\big)$ has a more complex dependence on the electrical parameters and the oscillator frequency. In fact, a parametric analysis with respect to r, H and C_r, shown in Fig. 9, reveals that the frequency (energy H) may have a significant impact on the instantaneous damping ratio, particularly when the oscillator trajectories diverge from the homoclinic orbit that separates intra-well from inter-well vibrations. Furthermore, there is a distinctive additional feature with respect to resistance. Although ζ_e for all cases is inversely proportional to R_L, Fig 9(b) shows that as $r \to 1$, the instantaneous damping ratio D_e is more sensitive to the oscillator energy, which may inflict considerably stronger dissipation per oscillation cycle with respect to the one expected from Case I. As r descreases, the effect of the frequency diminishes and the damping ratio asymptotically approaches the corresponding value of ζ_e from Cases I and II. For constant R_w (i.e. non-trivial α), this essentially means that the load resistance has an additional effect on damping compared with the previous two cases. The overall realised damping would then depend on the combined effect of R_L on the magnitude of ζ_e (given by Case I and Eq. (3)) and on the scaling factor of D_e in Eq. (15). Although the energy-dependent variations vanish as $r \to 0$, ζ_e is simultaneously increased leading to more robust damping values. This is a manifestation of the combined influence of the resistance R_L, which needs to be considered for VEH systems with RC shunts. On the other hand, if the total resistance $R_w + R_L$ is constant (i.e. the electrical damping ratio ζ_e is constant across all r's), variations of r lead to different values of R_w and, consequently, to considerable variations of α. In fact, as $r \to 1$ under constant ratio ζ_e, $\alpha \to 0$ and $D_e\big(\omega_s(H)\big) \to \zeta_e$, which is also true for $r \to 0$, revealing an intermediate critical value for r where damping is unfavourably maximised. Figure 9(c) shows the variation of D_e for selected energy values, where a maximum damping ratio is clearly realised. The effect of stronger dissipation is observed in the calculated mean crossing rate for this case in Fig. 10(a). It is observed that increasing r leads to less frequent crossings between wells, which however, does not necessarily lead to reduced mean power (see Fig 10(b)). The load voltage is proportional to resistance, which is shown from the almost linearly increasing power for $r \in (0.8, 0.9)$ where the crossing rate is almost constant. As soon as stronger dissipation is induced by higher values of r, the mean power saturates to maximum value, which is found very close to $r = 1$.

The above discussion reveals two different strategies for maintaining a low electrical damping ratio. Selecting the highest possible R_L ($r \to 1$) does not necessarily lead to optimal power output because of the damping alterations. In fact, the optimal resistance for power

generation stemming from Case I might have to be limited by ratio r such that damping remains sensible. For example, a value of $r = 0.8$ leads to nearly constant damping ratio across all energies and close to the value from Case I, whereas $r = 0.9975$ brings frequency-dependent variations up to 12 times. A strategy for maintaining stochastic resonance should therefore carefully consider the proportion of each resistor to mitigate excessive damping.

Furthermore, the capacitance may considerably affect energy dissipation. Observing Eq. (15), the influence of $r \to 1$ can be cancelled if $\alpha \gg \Omega(H)$, which can be configured with low values of C_r. Fig. 9(d),(e) show the damping ratio against C_r and H for $r = 0.9957$. It is observed that D_e is almost constant across the whole range of H, with the exception of trajectories near the homoclinic orbit where the value of the damping ratio asymptotically approaches ζ_e. Effectively the capacitance may cancel the in-cycle, energy-dependent fluctuations of the instantaneous damping ratio, as Fig. 9(e) shows; however, it can also lead to excessive overall disspation, as Fig. 10(b),(d) reveal. The capacitor is used to regulate the fluctuations of the rectifier voltage output. Moreover, an intuitive approach is to use this for energy storage as well, in order to mitigate potential shortages in the supply of the harvester. Nevertheless, increasing the capacitance may lead to dramatic damping ratios to the order of $\zeta_e/(1-r)$, which would adversely affect the amplitude of vibrations. Interestingly, the damping ratio remains relatively unaffected below a threshold value of C_r, which in the case study presented in Fig 9(d) is close to $10\mu F$. Monitoring the crossing rate and the corresponding mean power in a parametric analysis with respect to C_r shown in Fig. 10(b),(d), this critical capacitance is found to greatly affect the magnitude of the harvested power. A capacitance below the threshold can lead to strong stochastic resonance with amplified power output with respect to higher capacitance. Higher C_r may offer larger storage and better elimination of the voltage ripples, however, excessive capacitance can rapidly decrease the harvested power. This effectively can inform designers of a maximum C_r, which offers the largest energy storage capacity without dissipating the oscillator's stochastic resonance. Interestingly, the response at the critical capacitance not only maintains stochastic resonance, but it corresponds to optimal harvested power as well.

5 CONCLUSIONS

This paper has demonstrated the effect of the electrical load of a vibration energy harvester on the manifestation of stochastic resonance and the corresponding implications for harvested power. A numerical Path Integration method has been used to compute the joint response Probability Density Function of the harvester under various configurations and parameter variations. The mean crossing rate between the two wells of the bi-stable potential energy has been used as an indicator of the strength of stochastic resonance. It has been

shown that the optimal harmonic frequency has a nonlinear dependence on the system overall energy. Moreover, the indispensable usage of a rectifier and a capacitor has been shown to inflict considerable variations on the optimal electrical damping. The rectifier activation threshold weakens the electrical dissipation of the oscillator energy, which, although it leads to more frequent jumps between the wells, leads to lower average power extraction. Notably, the threshold value modifies the optimal load resistance for maximum power output. Furthermore, the addition of a capacitor to stabilise the voltage ripples and to act as energy storage has been found to level out fluctuations of the damping ratio when the rectifier conducts, whereas a maximum capacitance has been revealed for strong stochastic resonance. This capacitance also corresponds to the optimal combination of harvested power and energy storage, informing designers for the most favourable selection of capacitors.

REFERENCES

[1] A. Marin, J. Turner, D.S. Ha, S. Priya, Broadband electromagnetic vibration energy harvesting system for powering wireless sensor nodes, *Smart Mater. Struct.* 22 (2013), 075008.

[2] N.G. Stephen, On energy harvesting from ambient vibration, *J. Sound Vib.* 293 (2006), 409–425.

[3] A. Erturk and D.J. Inman, A Distributed Parameter Electromechanical Model for Cantilevered Piezoelectric Energy Harvesters, *J. Vibration Acoustics* 130 (2008), 041002 (15 pages).

[4] B.P. Mann and N.D. Sims, Energy harvesting from the nonlinear oscillations of magnetic levitation, *J. Sound and Vibration*, 319 (2009), 515-530.

[5] Yanxia Zhang, Yanfei Jin, Pengfei Xu, Dynamics of a coupled nonlinear energy harvester under colored noise and periodic excitations, *International Journal of Mechanical Sciences* 172 (2020) 105418.

[6] P. Alevras, S. Theodossiades and H. Rahnejat, Broadband energy harvesting from parametric vibrations of a class of nonlinear Mathieu systems, *Appl. Phys. Lett.* 110 (2017), 233901.

[7] P. Alevras, S. Theodossiades and H. Rahnejat, On the dynamics of a nonlinear energy harvester with multiple resonant zones, *Nonlinear Dyn* 92 (2018), 1271–1286.

[8] D. Yurchenko , A. Burlon , M. Di Paola , G. Failla , A. Pirrotta, Approximate Analytical Mean-Square Response of an Impacting Stochastic System Oscillator With Fractional Damping, *ASME J. Risk Uncertainty Part B*. Sep 2017, 3(3): 030903 (5 pages).

[9] A.H. Nayfeh and P.F. Pai, Linear and Nonlinear Structural Mechanics, Wiley, New York, 2004.

[10] R.L. Harne and K.W. Wang, A review of the recent research on vibration energy harvesting via bistable systems, *Smart Mater. Struct*. 22 (2013) 023001 (12pp).

[11] R. Masana, M.F..Daqaq, Relative performance of a vibratory energy harvester in mono- and bi-stable potentials, *J Sound and Vibration* 330 (2011) 6036–6052.

[12] M.F. Daqaq, Transduction of a bistable inductive generator driven by white and exponentially correlated Gaussian noise, *J Sound and Vibration* 330 (2011) 2554–2564.

[13] H. T. Zhu Probabilistic Solution of a Duffing-Type Energy Harvester System Under Gaussian White Noise, *ASME J. Risk Uncertainty Part B*. 2015, 1(1): 011005 (8 pages)

[14] I.A. Kougioumtzoglou, Y. Zhang; and M. Beer, Softening Duffing Oscillator Reliability Assessment Subject to Evolutionary Stochastic Excitation, *ASCE-ASME J. Risk Uncertainty Eng. Syst., Part A: Civ. Eng*., 2016, 2(2): C4015001

[15] C.R. McInnes, D.G.Gorman and M.P.Cartmell, Enhanced vibrational energy harvesting using nonlinear stochastic resonance, *J Sound and Vib* 318 (2008), 655-662.

[16] Luca Gammaitoni, Peter Hänggi, Peter Jung, and Fabio Marchesoni, Stochastic resonance, *Rev. Mod. Phys*. 70, (1998) 223.

[17] Rencheng Zheng, Kimihiko Nakano, Honggang Hu , Dongxu Su, Matthew P. Cartmell, An application of stochastic resonance for energy harvesting in a bistable vibrating system, *J Sound and Vibration* 333 (2014) 2568–2587.

[18] Y. Zhang, R. Zheng, K. Shimono, T. Kaizuka and K. Nakano, Effectiveness Testing of a Piezoelectric Energy Harvester for an Automobile Wheel Using Stochastic Resonance, *Sensors* 16 (2016), 1727 (16 pages).

[19] Hongjip Kim, Wei Che Tai, Jason Parker and Lei Zuo, Self-tuning stochastic resonance energy harvesting for rotating systems under modulated noise and its application to smart tires, *Mechanical Systems and Signal Processing* 122 (2019) 769–785.

[20] H. Kim, W.C. Tai and L. Zuo, Self-tuning stochastic resonance energy harvester for smart tires, *Proc. SPIE 10595, Active and Passive Smart Structures and Integrated Systems XII*, 105950U (16 March 2018).

[21] Z. Chen, B. Guo, Y. Xiong, C. Cheng and Y. Yang, Melnikov-method-based broadband mechanism and necessary conditions of nonlinear rotating energy harvesting using piezoelectric beam, *J. of Intelligent Material Systems and Structures* 27 (2016), 2555–2567.

[22] Zhang, Y., Zheng, R., Kaizuka, T. et al. Broadband vibration energy harvesting by application of stochastic resonance from rotational environments, *Eur. Phys. J. Spec. Top.* (2015) 224: 2687.

[23] Yanxia Zhang, Yanfei Jin, Stochastic dynamics of a piezoelectric energy harvester with correlated colored noises from rotational environment, *Nonlinear Dyn* (2019) 98:501–515.

[24] Wen-An Jiang, Li-Qun Chen, Stochastic averaging of energy harvesting systems*, Inter J Non-Linear Mechanics* 85 (2016) 174–187.

[25] Wen-An Jiang, Li-Qun Chen, Stochastic averaging based on generalized harmonic functions for energy harvesting systems, *J Sound and Vibration 377* (2016) 264–283.

[26] Ming Xu, Xiaoya Li, Stochastic averaging for bistable vibration energy harvesting system, *Inter J Mechanical Sciences* 141 (2018) 206–212.

[27] Tao Yang, Jiye Liu, Qingjie Cao, Response analysis of the archetypal smooth and discontinuous oscillator for vibration energy harvesting, *Physica A* 507 (2018) 358–373.

[28] Di Liu, Yanru Wu, Yong Xu, Jing Li, Stochastic response of bistable vibration energy harvesting system subject to filtered Gaussian white noise, *Mechanical Systems and Signal Processing* 130 (2019) 201–212.

[29] Yanxia Zhang, Yanfei Jin, and Pengfei Xu, Stochastic resonance and bifurcations in a harmonically driven tri-stable potential with colored noise, Chaos 29, 023127 (2019);

[30] Hui Zhang, Lawrence R. Corr, Tianwei Ma, Effects of electrical loads containing non-resistive components on electromagnetic vibration energy harvester performance, *Mechanical Systems and Signal Processing* 101 (2018) 55–66.

[31] Mohammed F. Daqaq, Rafael S. Crespo, Sohmyung Ha, On the efficacy of charging a battery using a chaotic energy harvester, *Nonlinear Dyn* (2020) 99:1525–1537.

[32] Quanqi Dai and Ryan L Harne, Investigation of direct current power delivery from nonlinear vibration energy harvesters under combined harmonic and stochastic excitations, *Journal of Intelligent Material Systems and Structures* 29(4), 2018, 514–529.

[33] Quanqi Dai and Ryan L Harne Charging power optimization for nonlinear vibration energy harvesting systems subjected to arbitrary, persistent base excitations, Smart Mater. Struct. 27 (2018) 015011

[34] P. Hänggi, P. Talkner, M. Borkovec, Reaction-rate theory: fifty years after Kramers, Rev. Mod. Phys. 62 (1990) 251–341.

[35] Dennis J. Tweten, Brian P. Mann, Experimental investigation of colored noise in stochastic resonance of a bistable beam, Physica D 268 (2014) 25–33.

[36] D Yurchenko, A Naess, P Alevras Pendulum's rotational motion governed by a stochastic Mathieu equation, Probabilist Eng Mech 31 (2013), 12-18.

[37] P. Alevras, D. Yurchenko, GPU computing for accelerating the numerical Path Integration approach, *Computers and Structures* 171 (2016) 46–53.

[38] A. Naess, V. Moe, Efficient path integration methods for nonlinear dynamic systems, *Probabilist Eng Mech* 15 (2000) 221–231.

[39] I Petromichelakis, A.F. Psaros, I.A. Kougioumtzoglou, Stochastic response determination and optimization of a class of nonlinear electromechanical energy harvesters: A Wiener path integral approach, *Probabilist Eng Mech* 53 (2018) 116–125.

[40] I.A. Kougioumtzoglou, P.D. Spanos, An analytical Wiener path integral technique for non-stationary response determination of nonlinear oscillators, Probabilistic Engineering Mechanics 28 (2012) 125–131.

[41] C. Zhang, R.L. Harne, B. Li, and K.W. Wang (2019). Statistical quantification of DC power generated by bistable piezoelectric energy harvesters when driven by random excitations. *Journal of Sound and Vibration* 442 (2019) 770-786.

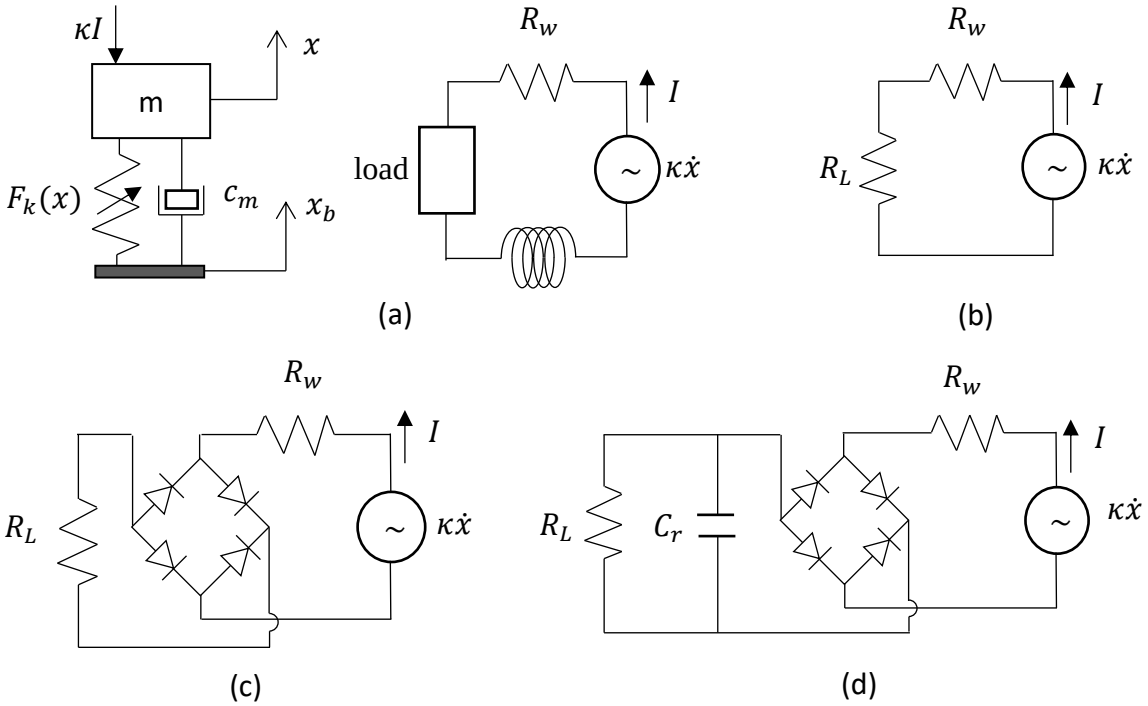

Fig. 1. (a) Schematic of the mechanical bi-stable oscillator and the coupled electric circuit; (b) simplified purely resistive electrical load corresponding to Case I; (c) circuit with rectifier depicting Case II; (d) rectified power with stabilising capacitor (Case III).

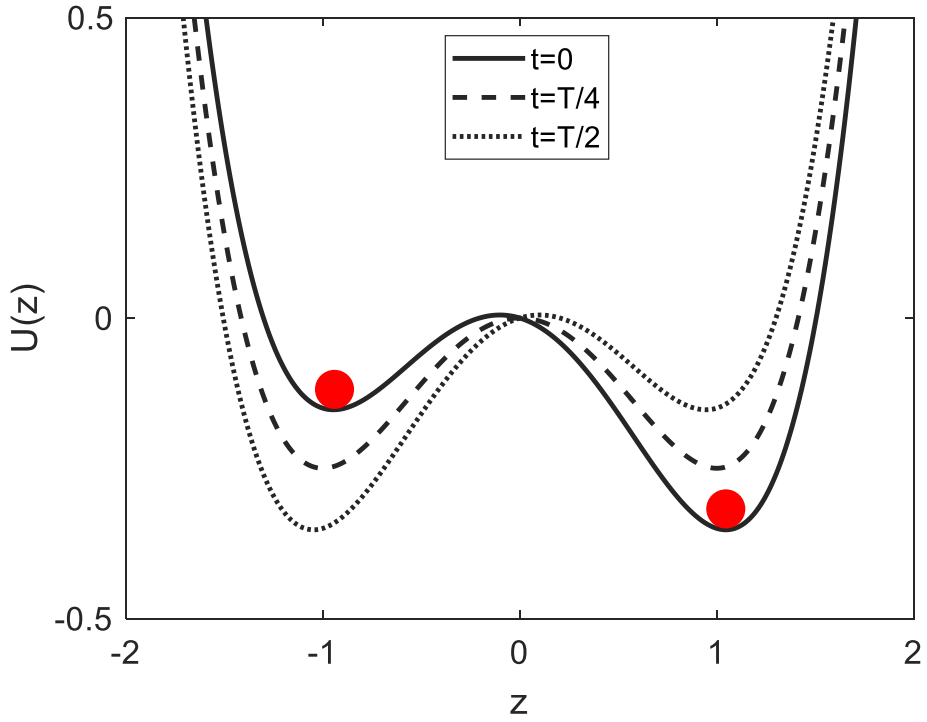

Fig. 2. Modulations of the bi-stable potential energy $U(z)$ by a weak periodic signal of period T.

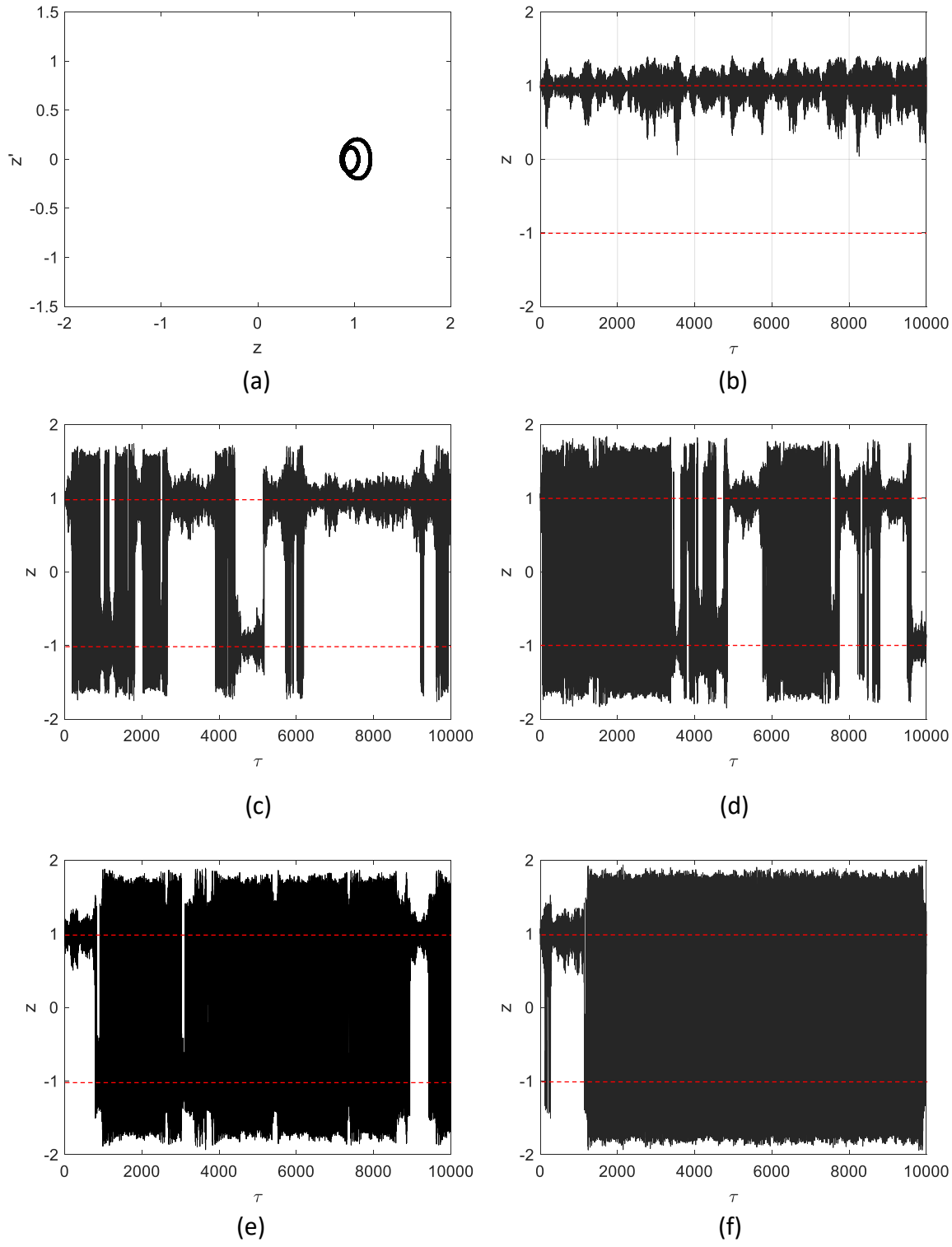

Fig. 3. Samples of the displacement response of the bi-stable harvester governed by Eq. (2) with stable equilibria at $z = \pm 1$ shown by dashed red lines. (a) Deterministic phase space plot for $\omega = 0.7$ and $\omega = 1.0$; (b) wideband excitation with $D = 0.001$; and response to combined harmonic with wide-band excitation for $D = 0.001$ and: (c) $\omega = 0.7$; (d) $\omega = 0.8$; (e) $\omega = 0.9$; (f) $\omega = 1.0$.

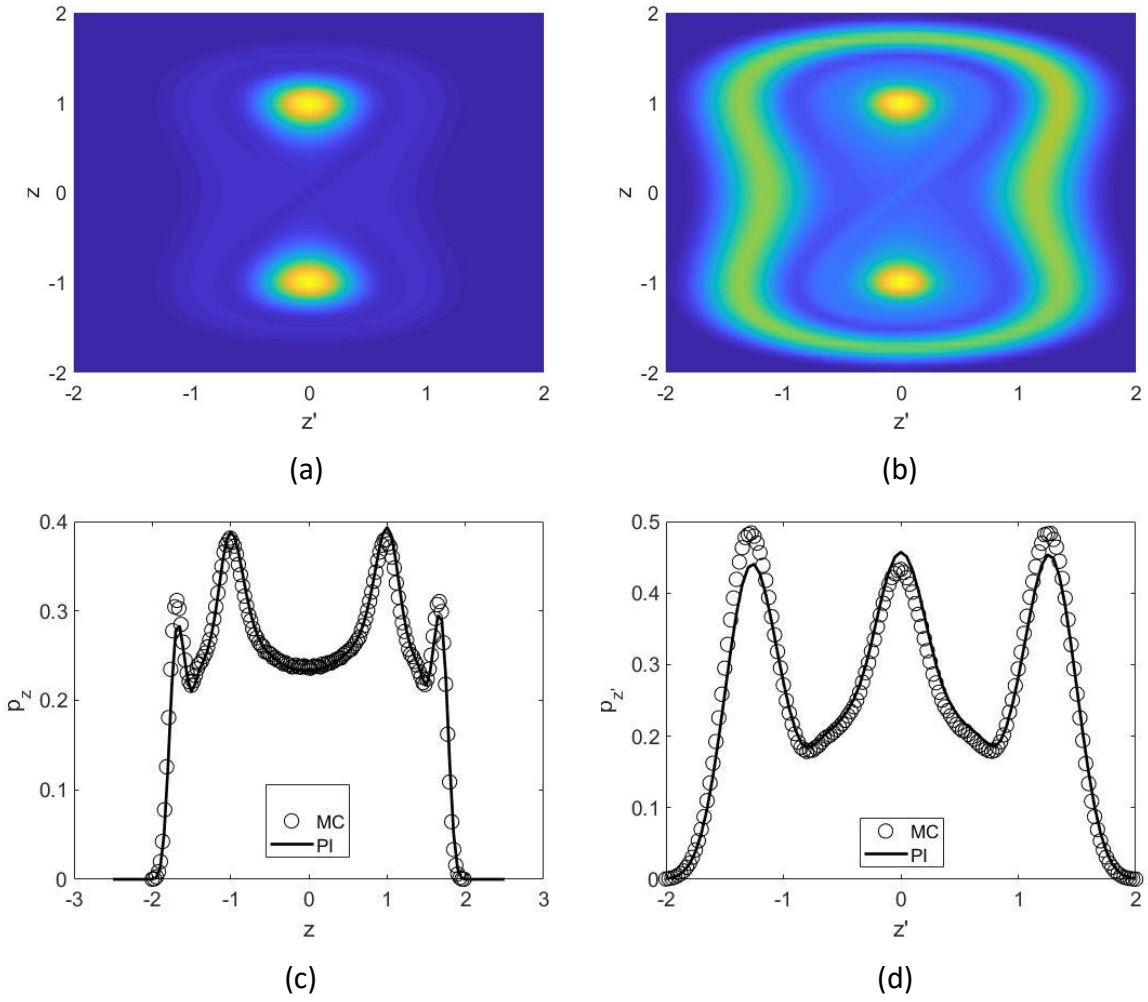

Fig. 4. Joint response PDF, $p_{zz'}$, for $A_n = 0.1$, $D = 0.001$ and (a) $\omega = 0.7$; (b) $\omega = 1.0$; comparison of (c) p_z and (d) $p_{z'}$ against MC simulations (1,000 samples) for $\omega = 1.0$;

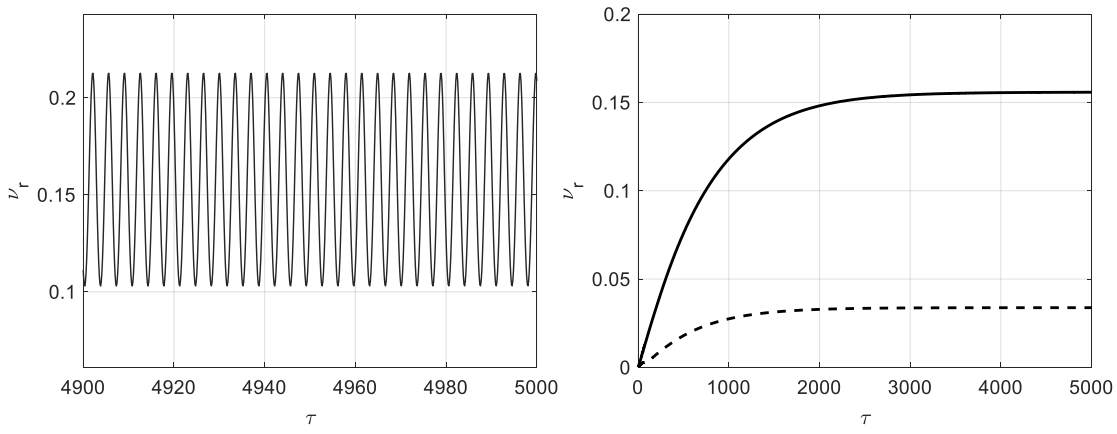

(a) (b)

Fig. 5. (a) Stationary time history of the crossing rate, ν_r, for A_n=0.08 and ω=0.9; (b) Complete time history of the moving mean of the crossing rate averaged over one period for $A_n = 0.08$ and $\omega = 0.9$ (————); $A_n = 0.05$ and $\omega = 0.75$ (– – – – –).

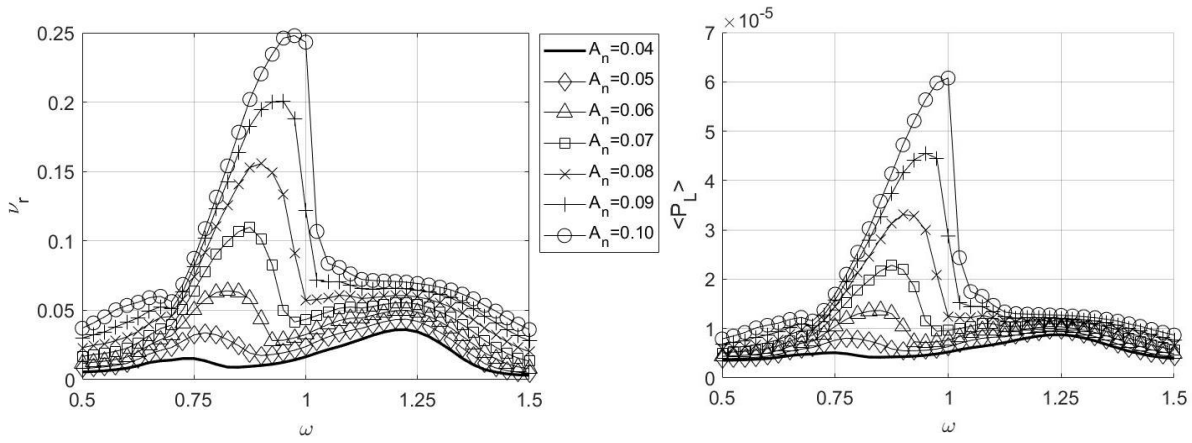

(a) (b)

Fig. 6. (a) Crossing rates for Case I with $R_L = 17\ \mathrm{k}\Omega$ and $D = 0.001$ for varying A_n; (b) corresponding mean power output

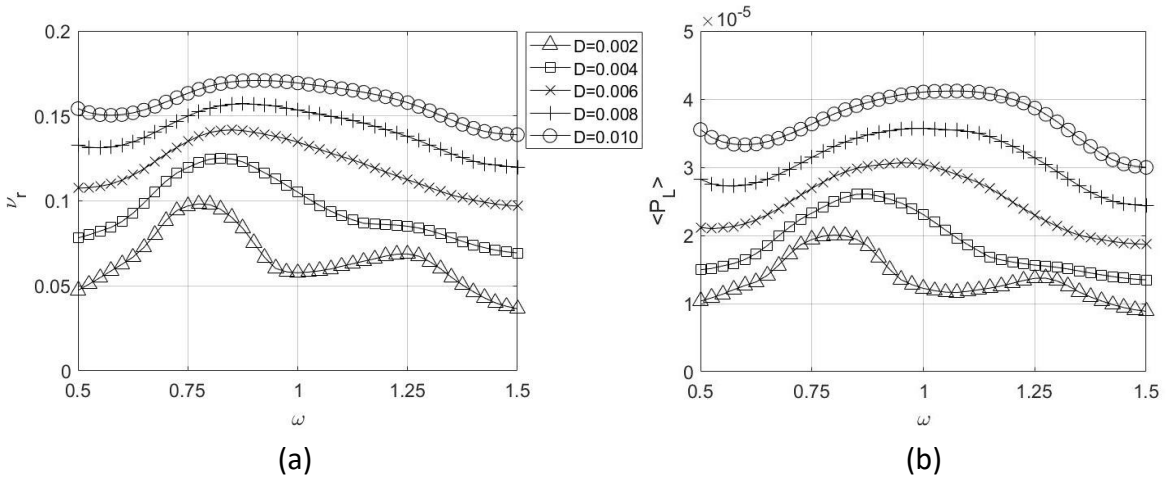

(a) (b)

Fig. 7. (a) Crossing rates versus harmonic excitation frequency for Case I with $R_L = 17\ \mathrm{k}\Omega$ and $A_n = 0.05$ for varying D as per the displayed legend; (b) corresponding mean power output.

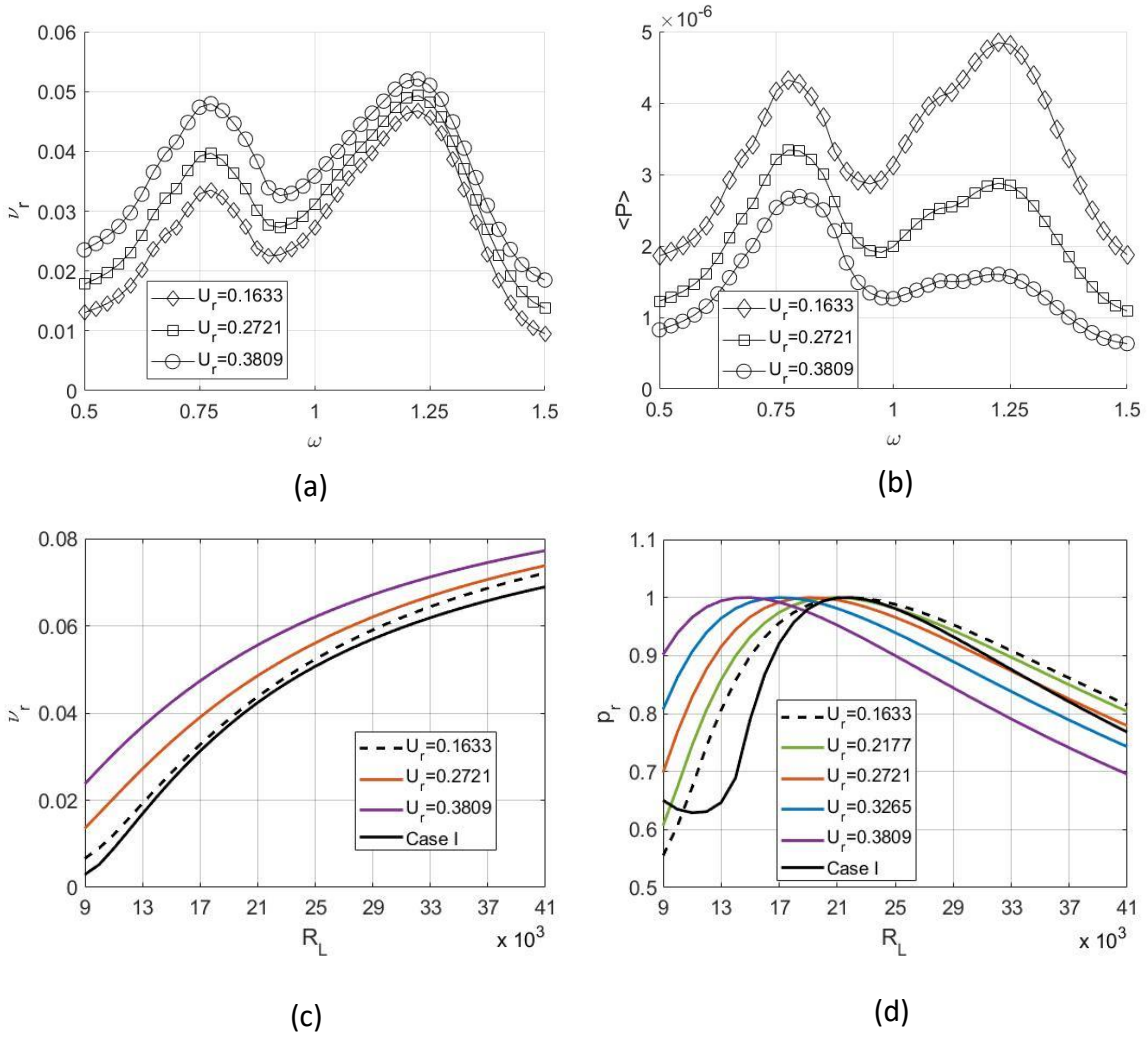

Fig. 8. (a) Crossing rates versus harmonic excitation frequency for Case II with $R_L = 17\ \mathrm{k}\Omega$ and $A_n = 0.05$ for varying rectifier threshold U_r as per the displayed legends; (b) corresponding mean power output. (c) Crossing rates and (d) mean power output against load resistance for various values of the rectifier voltage drop and $A_n = 0.05$, $\omega = 0.775$.

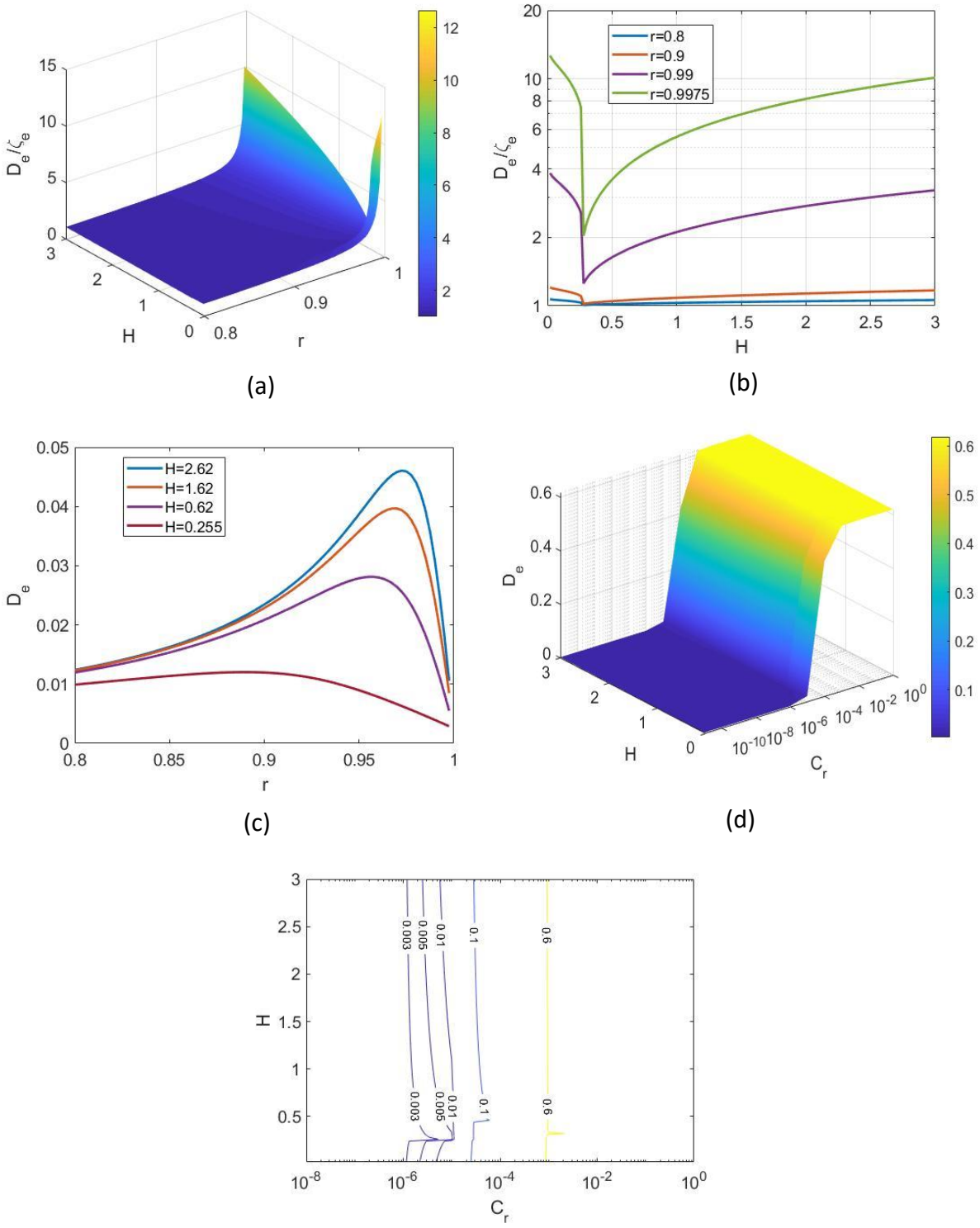

Fig. 9. Parametric variation of the damping ratio D_e with respect to: (a) resistance ratio r and energy H for $C_r = 10^{-5}$ F; (b) energy H for selected r values; (c) resistance ratio r under constant ζ_e; (d) capacitance C_r and energy H for $r = 0.9959$ and: (e) contour plot of D_e.

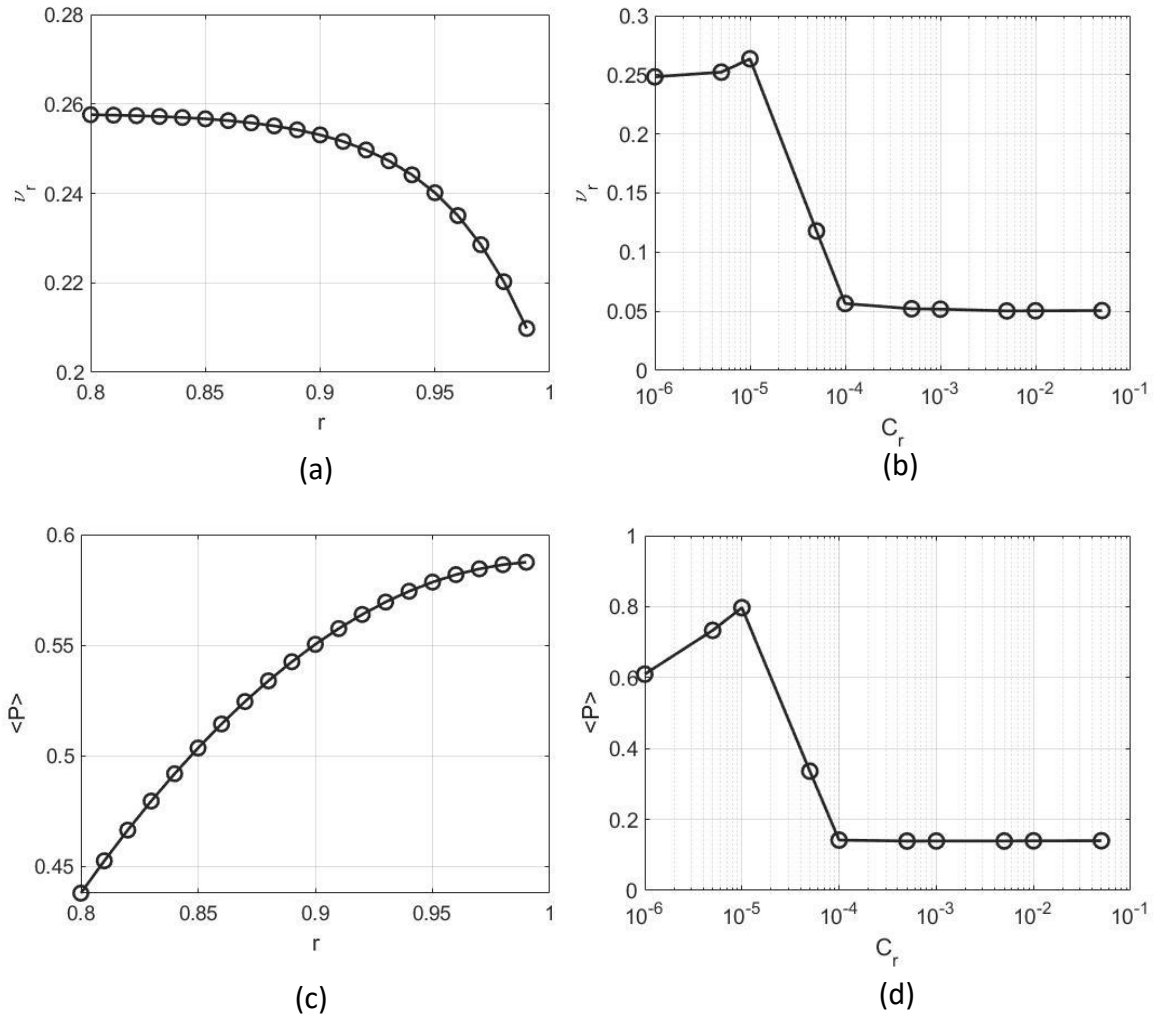

Fig. 10. Mean crossing rate ν_r (a),(b) and mean power $\langle P \rangle$ (c),(d) corresponding to Case III and Eqs (14) and (15) against resistance ratio r (left column) and capacitance C_r (right column).